Anomalous spin dynamics in a two-dimensional magnet induced by anisotropic critical fluctuations

Zefang Li,[1,2] Dong-Hong Xu,[1,2] Xue Li,[1,2] Hai-Jun Liao,[1,3] Xuekui Xi,[1] Yi-Cong Yu,[4,*] and Wenhong Wang[1,3,†]

[1]*Beijing National Laboratory for Condensed Matter Physics, Institute of Physics, Chinese Academy of Sciences, Beijing 100190, China*

[2]*University of Chinese Academy of Sciences, Beijing 100049, China*

[3]*Songshan Lake Materials Laboratory, Dongguan, Guangdong 523808, China*

[4]*State Key Laboratory of Magnetic Resonance and Atomic and Molecular Physics, Wuhan Institute of Physics and Mathematics, APM, Chinese Academy of Sciences, Wuhan 430071, China*

(Received 13 May 2022; revised 1 August 2022; accepted 2 August 2022; published 22 August 2022)

We investigate the temperature dependence of g factor in two-dimensional (2D) ferromagnet $CrSiTe_3$ by combining three-dimensional vector-ferromagnetic resonance (FMR) experiments. It is shown from the angular dependence that the dramatic g shift near critical temperature originates from the interplay of enhanced magnetic fluctuations and anisotropic spin interactions in 2D magnetism. The crossover from isotropic to anisotropic g factor for $T \to T_c$ yields anomalously parallel pumped excitations. In the critical regime, the field suppression of critical fluctuations is associated with the field dependence of g shift. Furthermore, the results of FMR g shift are scaled by susceptibilities and spontaneous magnetization obtained from magnetometry measurements, which show good agreement with the universality class of the 2D Ising model.

DOI: 10.1103/PhysRevB.106.054427

I. INTRODUCTION

In the vicinity of the critical point, fluctuations and correlations drive abundant phase transitions and critical phenomena, which depend heavily on dimensionality. In particular, the intrinsic 2D van der Waals (vdW) magnetism undergoes enhanced magnetic fluctuations from the Ginzburg criterion [1], as well as strong anisotropic spin interactions for ruling out the Mermin-Wagner theorem [2]. While Cr-based 2D materials emerge with complex interplay of microscopic interactions involving Heisenberg, 2D Ising, XY, and Kitaev models [3–6], the tuning of external perturbations like strain, light, gating, and magnetic field can efficiently control the magnetic fluctuations and further manipulate various novel physical states [7], including the quantum spin liquids [4], superconductivity [8], atomic 2D magnetism [9], and so on. Therefore, unveiling magnetic fluctuations and microscopic interaction are significant for understanding the mechanisms which lead to phase transitions in 2D systems.

Ferromagnetic resonance provides high sensitivity and resolution of resonance spectra. The information extracted from spectra includes line shift and linewidth, which are determined by the imaginary part of the dynamical spin susceptibility $\chi''(q = 0, \omega, H)$. In general, the anisotropic spin interactions generate magnetic anisotropy and decide the line shift. And, magnetic fluctuations are related to the linewidth, which increases anomalously near T_c because of the divergent nature of the random torque [10]. However, in order to stabilize 2D magnetism at finite temperature, magnetic anisotropy is important for combating magnetic fluctuations. Especially in the critical regime around T_c, longitudinal fluctuations are suppressed and rotational invariance is destroyed, which will bring modified static critical behavior [11] and dramatic changes in the spin dynamics [12]. On the one hand, when T_c is approached from the paramagnetic phase, Nagata *et al.* introduced a theoretical concept for the electron paramagnetic resonance (EPR) line shift in low-dimensional magnet, or equivalently, the g shift which satisfies with the scaling of static magnetic susceptibility χ [13–16]. The Nagata theory indicates that beyond the spin-orbital coupling-induced g shift at zero field, a correction of g shift under high-temperature perturbation approximation and in the presence of finite magnetic field should be considered for the studies of critical phenomena in low-dimensional magnet. On the other hand, in the ferromagnetic phase below T_c, since the large anisotropy field is contributing the line shift, the accurate analysis of g shift thus requires a large set of angular- and frequency-dependent data. Generally, the critical region is restricted in the extreme vicinity of T_c for 3D magnets. Due to large Ginzburg number for 2D magnets, the widening of the critical region offers the possibility to detect significant g shift. However, probably due to the lack of complete theory of critical dynamics below T_c, previous reported g shift in the ferromagnetic state of 2D materials is not yet clearly explained [17,18].

To attack this problem, here we carry out 3D-vector ferromagnetic resonance (FMR) experiments for the precise determination of g factor upon 2D vdW magnet $CrSiTe_3$ (CST) above and below T_c. There are several reasons for choosing CST as a template: (i) The magnetic correlations in $CrSiTe_3$ exhibit quasi-2D Ising ferromagnetic behavior even in bulk counterpart [19], while the structural-related $CrGeTe_3$ (CGT) is a good reference compound close to classical Heisenberg behavior [9]. (ii) Strong critical fluctuations around T_c have been supported by neutron scattering [19],

*ycyu@wipm.ac.cn

†wenhong.wang@iphy.ac.cn

which decay exponentially when deviating from T_c. (iii) The localized magnetism arises from the Cr^{3+} ions that are located at octahedral crystal field with nearly quenched orbital moment ($L \approx 0$), and thus predicts a spin-only magnetic moment 3.87 μ_B/Cr and a quasi-isotropic g factor near 2. Above all, CST satisfies typical 2D correlations, strong critical fluctuations, and a quasi-isotropic g factor in normal state. Therefore, the experimental observation of the deviation of a temperature- and angular-dependent g factor near T_c will be solid evidences for anisotropic critical fluctuations.

II. EXPERIMENT METHOD

Bulk CST and CGT single crystals were grown by the self-flux method [20]. The magnetization was characterized in a Quantum Design magnetic property measurement system. The sample was cut into a rectangular prism, of which the demagnetizing tensor can be calculated [21].

Broadband 3D vector-ferromagnetic resonance experiments were carried out on a homemade coplanar waveguide sample rod, which was adapted to the Cryogenic vector magnet systems. FMR spectra were recorded with a vector network analyzer (ZVA 40, Rohde & Schwarz) in transmission mode (S12) over a frequency range of 1–40 GHz, in response to the scanning of magnetic field with the rate of 50 Oe/s. The resonance field was determined by asymmetric Lorentzian fit to the spectra.

III. RESULTS AND DISCUSSION

A. Critical spin dynamics in low-dimensional magnet

The theories of static and dynamic critical behavior of magnetic systems have been well established, such as Ginzburg-Landau theory, renormalization group, and mode-coupling theory [22]. However, most of the applications to EPR experiment focus on the critical broadening of linewidth, which is associated with the magnetic relaxation at zero wave vector and finite frequency. The most successful theory of EPR line shift in anisotropic magnet is proposed by Nagata *et al.* [13–16], which is based on the classical spin approximation and gives a simple form of eigenfrequency:

$$\hbar\omega = \frac{\langle [S^-, [S^+, \mathcal{H}]]\rangle}{2\langle S^\xi\rangle}, \tag{1}$$

where $S^\pm = \sum_j S_j^\eta \pm iS_j^\upsilon$ are the transverse components of spins, and $S^\xi = \sum_j S_j^\xi$ is the longitudinal spins which point along the internal effective field $H_{\rm eff}$. The global $\{\eta, \nu, \xi\}$ basis is defined by the quantization axis along $H_{\rm eff}(\theta_H, \varphi_H)$. The global $\{x, y, z\}$ basis is defined by the crystal axis. This expression can also be derived from the Fourier transformation of the imaginary part of the dynamical spin susceptibility, which corresponds to the phenomenological result given by Huber *et al.* [23]. In order to ensure the quantization axis defined by the internal effective field $H_{\rm eff}$ to be consistent with the external static field H, the application of Eq. (1) requires weak magnetic anisotropy, which is generally satisfied in paramagnetic state. However, in ferromagnetic state, regardless of the magnetocrystalline field, we can treat the $H_{\rm eff}$ as nearly parallel to H when above the saturation field. Therefore, as will be seen, we can extend Nagata theory to the ferromagnetic state below T_c because the g shift only depends on the slope of ω–H, and has nothing to do with the intercept of ω–H associated with the magnetocrystalline field.

As for the uniaxial ferromagnet $CrSiTe_3$, let us consider a generalized Heisenberg spin Hamiltonian [24,25]:

$$\mathcal{H} = -\frac{1}{2}\sum_{\langle j,l\rangle}\left(JS_jS_l + \Lambda S_j^z S_l^z\right) - \sum_j AS_j^z S_j^z - \mu_B Hg\sum_j S_j. \tag{2}$$

The first term corresponds to the Heisenberg isotropic exchange J and the anisotropic symmetric exchange Λ. The second term is the additional single-ion anisotropy term A, and the last term corresponds to the Zeeman energy. We put the Hamiltonian into Eq. (1) and assume no in-plane anisotropy $\langle S^\eta S^\eta\rangle = \langle S^\upsilon S^\upsilon\rangle$:

$$\hbar\omega(\theta_H) = g_{\rm iso}\mu_B H_{\rm eff} + \sum_{j,l}\frac{\hbar^2(3\cos^2\theta_H - 1)}{\langle S^\xi\rangle} \times\left(\frac{1}{2}\Lambda + A\right)\langle S^\xi S^\xi - S^\eta S^\eta\rangle. \tag{3}$$

Consider the finite-temperature case $\beta = 1/k_BT$, in which the mean values of the operators can be evaluated by the partition function $Z = {\rm Tr}\, e^{-\beta\mathcal{H}}$:

$$\langle S^\xi\rangle = \frac{{\rm Tr}[e^{-\beta H_0 - \beta H_f}S^\xi]}{{\rm Tr}[e^{-\beta H_0 - \beta H_f}]} \simeq \frac{{\rm Tr}[e^{-\beta H_0}(1 - \beta H_f)S^\xi]}{{\rm Tr}[e^{-\beta H_0}]}, \tag{4}$$

where $\mathcal{H} = H_0 + H_f$ and $H_f \doteq g_{\rm iso}\mu_B H_{\rm eff}S^\xi \ll k_BT$. Then, we have $\langle S^\xi\rangle = -\beta g_{\rm iso}\mu_B H_{\rm eff}\langle\langle S^\xi S^\xi\rangle\rangle$, where " $\langle\langle\circ\rangle\rangle$" means average in zero field. Therefore, the line shift at finite temperature is given by

$$\hbar\omega(\theta_H) = g_{\rm iso}\mu_B H_{\rm eff} + \frac{g_{\rm iso}\mu_B H_{\rm eff}(3\cos^2\theta_H - 1)}{2k_BT\langle\langle S^\xi S^\xi\rangle\rangle} \times\left(\frac{1}{2}\Lambda + A\right)\sum_{jlkm}\left\langle\left\langle\left(S_j^\xi S_l^\xi - S_j^\eta S_l^\eta\right)S_k^\xi S_m^\xi\right\rangle\right\rangle, \tag{5}$$

where the four spin correlation function $\langle\langle(S_j^\xi S_l^\xi - S_j^\eta S_l^\eta)S_k^\xi S_m^\xi\rangle\rangle$ refers to the fluctuations of correlated spins. On the one hand, the isotropic component J of total spin Hamiltonian is SU(2) invariant and conserves the magnetic moment, which contributes a δ-function resonance and does not impose any angle-dependent feature. On the other hand, the noncommuting anisotropic components Λ and A are responsible for line shift, which can be identified by angle-dependent measurements. If we further define $g(\theta_H) = \hbar\omega(\theta_H)/(\mu_B H_{\rm eff})$, then from Eq. (5) we get the expression for the anisotropic g factor:

$$g(\theta_H) = \Delta g(3\cos^2\theta_H - 1) + g_{\rm iso}. \tag{6}$$

To understand the magnetic torque dynamics near T_c, Fig. 1(a) illustrates schematically the rectangular-shaped single crystal placed in a coplanar waveguide where it is acted upon by an alternating magnetic field $H_{\rm rf}$. In response to scanning of a static magnetic field H at right angles, resonance absorption signals can be detected in the case that $\omega = \gamma H_{\rm eff}$, where $\gamma = g\mu_B/\hbar$ is the gyromagnetic ratio and $H_{\rm eff}$ is the effective internal field. When resonance occurs,

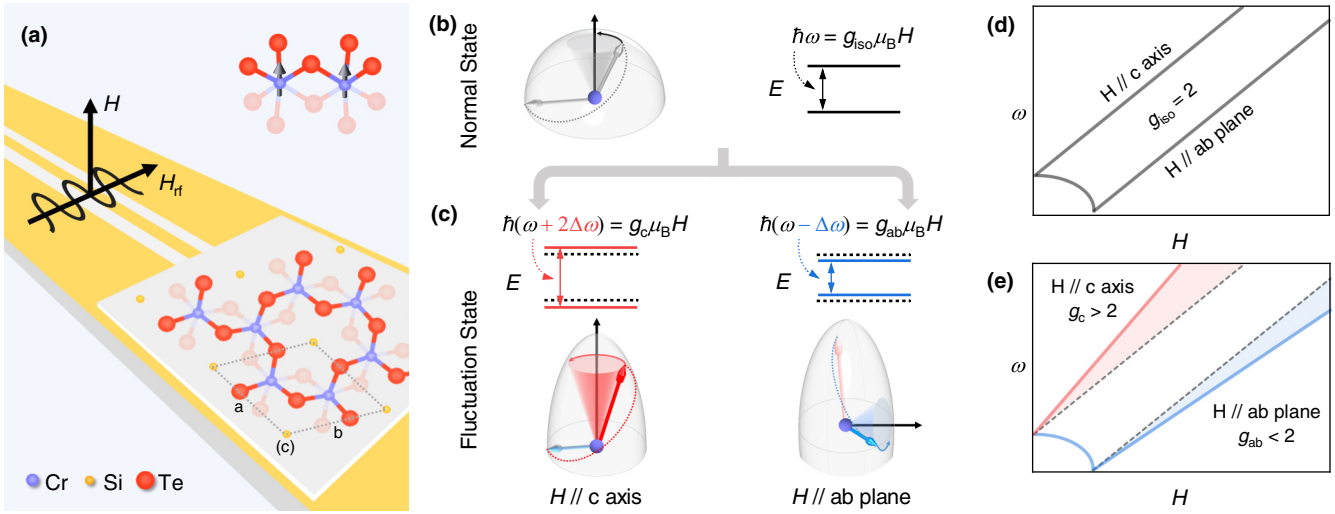

FIG. 1. (a) Schematic illustration of the 3D vector-FMR experiment. The top inset shows the magnetic ion Cr^{3+} surrounded by a distorted octahedral crystal field with an out-of-plane arrow representing its easy magnetization direction. (b), (c) Illustration of the anisotropic g factor, the shifts of energy diagrams, as well as the magnetic torque dynamics around an effective magnetic field in normal and fluctuation state. (d), (e) FMR spectra above the saturation field will give parallel straight lines along easy ($\boldsymbol{H} \parallel \boldsymbol{c}$ axis) and hard ($\boldsymbol{H} \parallel \boldsymbol{ab}$ plane) direction for isotropic $\boldsymbol{g}_{iso} = 2$, in contrast to the unparallel behavior for anisotropic $\boldsymbol{g}_c > 2$ and $\boldsymbol{g}_{ab} < 2$.

the spontaneous magnetization M_s induces Larmor precession along the effective field direction. As shown in Fig. 1(b), in normal state the Zeeman splitting ($g_{iso} = 2$) is independent of orientation. And, FMR spectra above the saturation field [Fig. 1(d)] will give parallel straight lines along the easy ($H \parallel c$-axis) and hard ($H \parallel ab$-plane) direction. In fluctuation state, Eq. (6) indicates the g shift along easy axis Δg_c is twice the value along the hard plane Δg_{ab}. Therefore, FMR spectra above the saturation field [Fig. 1(e)] will show the upwards- or downwards shifts of the slopes, which clearly indicate the g shift.

B. Temperature dependence of g shift

We obtain the temperature dependence of g factor by measuring FMR spectra above and below the critical temperature $T_c = 34.15$ K. The applied magnetic field, plotted in Fig. 2(a), is perpendicular to the direction of the rf field for both in-plane and out-of-plane directions. As shown in Fig. 2(b), the resonance frequency $\omega(H)$ at varied temperatures shows two distinct unparallel features in high fields around T_c. The slopes of $\omega - H$, as the analytical expression given by the Smit-Beljers approach [26], directly represent the gyromagnetic ratio γ (or g factor):

$$\left(\frac{\omega}{\gamma}\right)^2 = [H + N'(\theta_H)M_s + H_A\cos^2\theta_H] \times [H + N''(\theta_H)M_s + H_A\cos 2\theta_H], \quad (7)$$

where $N'(\theta_H) = N_x - N_y\sin^2\theta_H - N_z\cos^2\theta_H$ and $N''(\theta_H) = (N_y - N_z)\cos 2\theta_H$ represent the effective shape demagnetization factor (N_x, N_y, and N_z represent the shape demagnetization factor of the rectangular crystal), M_s is the spontaneous magnetization, θ_H is the angle between H and z axis, and $H_A = 2K/M_s$ is the anisotropic field (K is the magnetocrystalline anisotropy). It should be noted that Eq. (7) is only

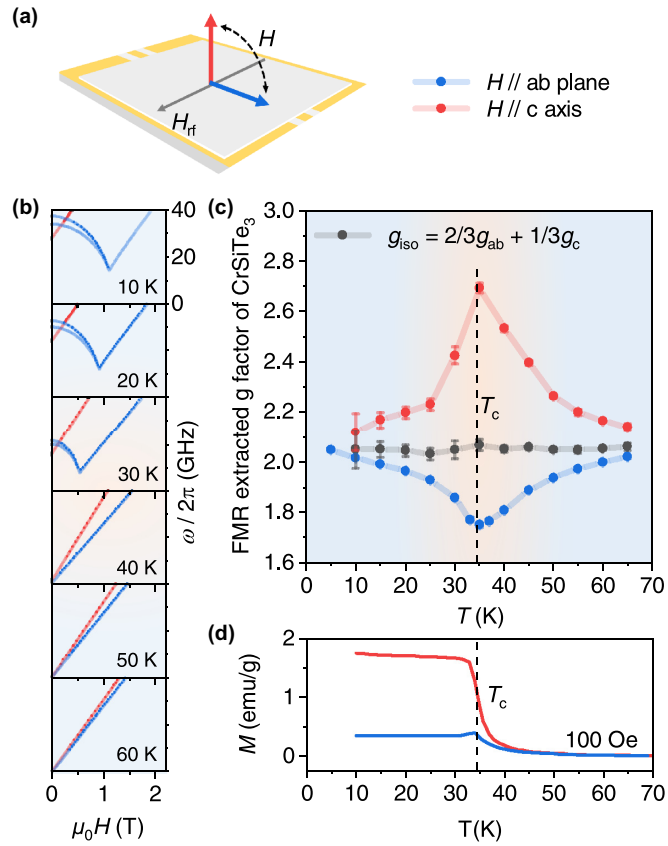

FIG. 2. (a) Geometrical configuration of FMR experiment for in-plane (blue) and out-of-plane directions (red). (b) FMR spectra above and below the critical temperature. (c) Comparison of the temperature-dependent g factor extracted from FMR data above saturation field. Calculation of isotropic component $\boldsymbol{g}_{iso} = 2/3\boldsymbol{g}_{ab} + 1/3\boldsymbol{g}_c$ is basically in line with the spin-only value of $\boldsymbol{g} = 2$. (d) Temperature dependence of magnetization under 100 Oe magnetic field showing the Curie temperature $\boldsymbol{T}_c = 34.15$ K.

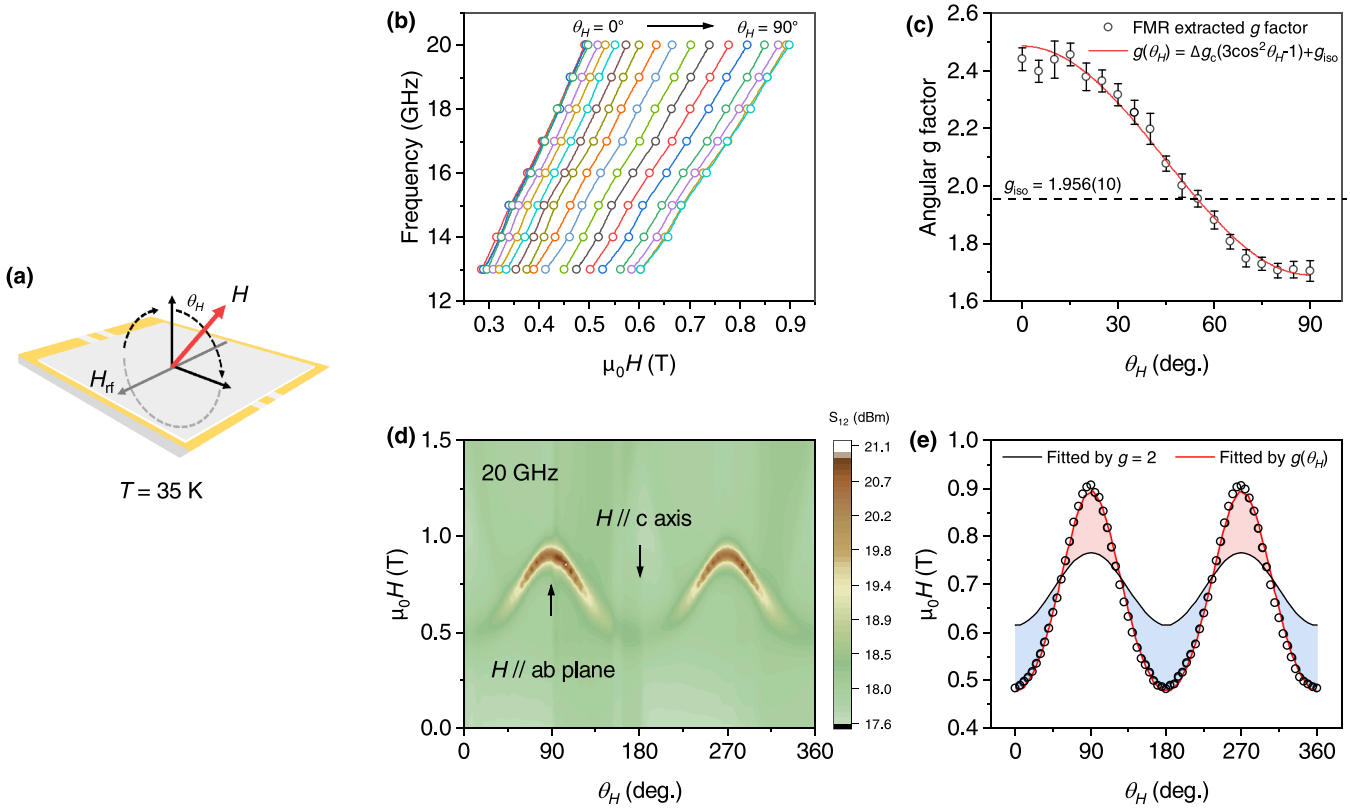

FIG. 3. (a) Geometrical configuration of 3D vector-FMR experiment measured at fixed temperature $\boldsymbol{T} = 35$ K. (b) Angular dependence of FMR spectra from 13 to 20 GHz. (c) Angular dependence of the extracted g factors. The red line is fitted by $\boldsymbol{g}(\theta_{\boldsymbol{H}}) = \boldsymbol{\Delta g}(3\cos^2\boldsymbol{\theta_H} - 1) + \boldsymbol{g}_{\rm iso}$. (d) Experimentally measured angular-dependent FMR spectra at 20 GHz. (e) Simulated resonance field using spin-only value $\boldsymbol{g} = 2$ (black) and angular value $\boldsymbol{g}(\theta_{\boldsymbol{H}})$ (red). The differences indicate the additional line shift is contributed by critical fluctuations, which vanish at the magic angle ($\theta_{\boldsymbol{H}} = 54.74^\circ$).

valid well above the saturation field, approximately when $H \parallel M_s$. We next determine the temperature evolution of g factor in Fig. 2(c). The clear downwards- or upwards shifts of the g factor, with a maximum value at T_c, are observed at varied temperature. Based on Eq. (6), the isotropic component $g_{\rm iso}$ (black) can be determined by $g_{\rm iso} = 2/3g_{ab} + 1/3g_c$, which is basically in line with the spin-only value of $g = 2$.

It is important to note that g shift arises from both amplitudes of critical fluctuations and anisotropic exchange interactions. Compared with the structural related CGT with higher $T_{\rm c} \approx 68$ K and quasi-isotropic Heisenberg spin models, the g shift of CST [$\Delta g_{\rm c}(35\,{\rm K}) \approx 0.70$] is much larger than that of CGT [$\Delta g_{\rm c}(70\,{\rm K}) \approx 0.20$] (See Supplemental Material [27]), even though the thermal energy kT at critical temperature of CGT is almost twice that of CST. Due to that anisotropic symmetric exchange Λ is much smaller in CGT, the g shift of CGT is restricted to a small temperature window near T_c. Interestingly, CGT has been confirmed to exhibit long-range FM order the on atomic scale [9], while the lack of evidence on stable FM order in atomic CST layers can be predicted by strong spin fluctuations observed in our FMR experiment. Therefore, the precise determination of g shift in 2D magnet, which is associated with anisotropic critical fluctuations, provides us a sensitive method for screening atomic 2D magnet candidates from bulk counterparts.

C. Angular dependence of g shift

As shown in Fig. 3(a), in order to determine the angular-dependent gf actor at T_c, we next perform FMR experiments by rotating the static magnetic field H while keeping $H \perp H_{\rm rf}$. As shown in Figs. 3(b) and 3(c), the angular g factors are extracted by multifrequency measurements from 13 to 20 GHz. The $(3\cos^2\theta - 1)$-like angular dependence fits well with the FMR extracted g factors, where the magic angle with a spin-only g factor is observed at $\theta_H = 54.74^\circ$.

Furthermore, it is widely accepted that angular-dependent FMR provides precise analysis of magnetic anisotropy [10]. As one of the representative examples on 2D magnet, Lee *et al.* came up with a symmetry-based theoretical analysis on fundamental spin interactions in CrI_3 [28]. However, the above modelings are all based on the given isotropic g factor, in other words, an isotropic Zeeman splitting in the general Hamiltonian or free-energy function. Here, we provide insight into the additional line shift contributed by angular-dependent g factor. Figure 3(d) shows the experimentally measured angle-dependent FMR spectra at 20 GHz and 35 K. In Fig. 3(e), we find that only by substituting the extracted $g(\theta_H)$ from Fig. 3(c), the simulated H from Eq. (7) can match well with the experimental result. In contrast, the isotropic $g_{\rm iso} = 2$ is insufficient for explaining the additional line shift. The shifts of resonance field between $g(\theta_H)$ and $g_{\rm iso}$ clearly show the additional anisotropy contributed by anisotropic critical fluctuations.

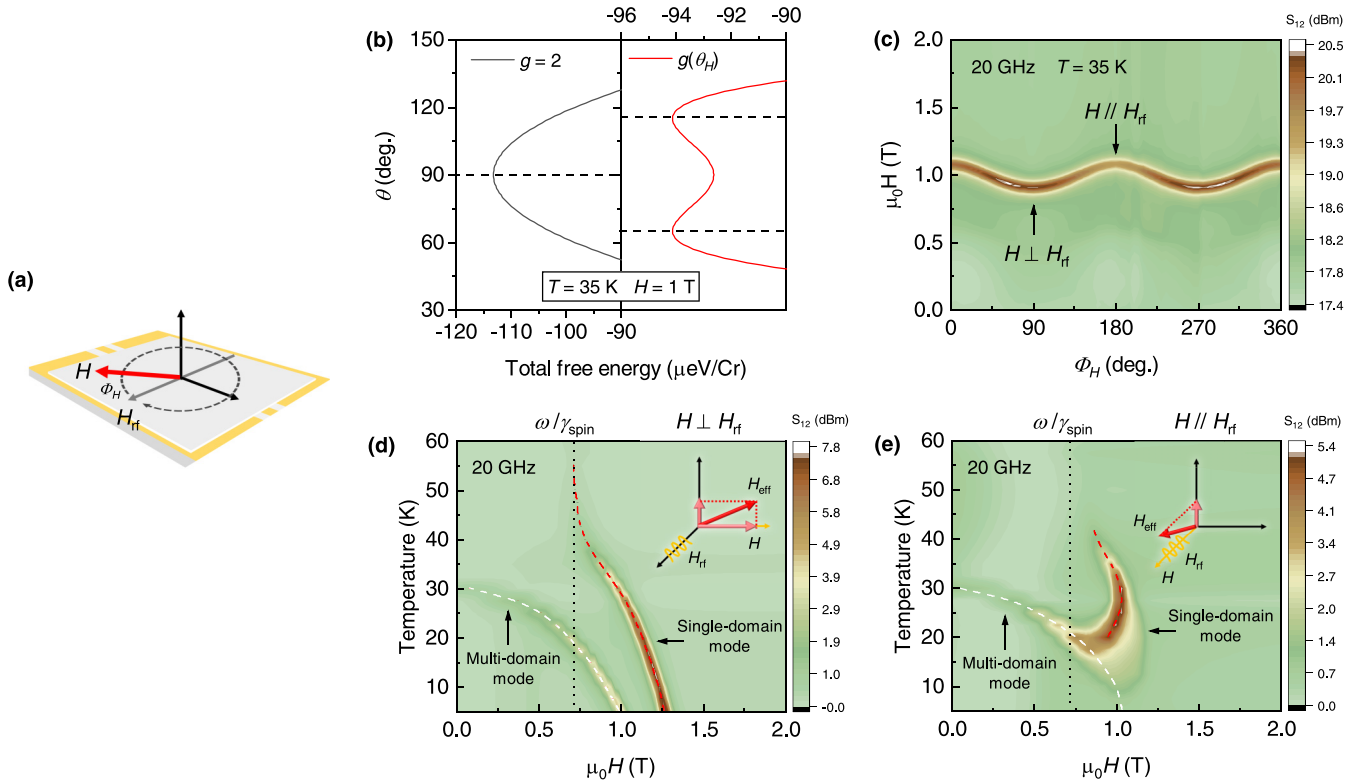

FIG. 4. (a) Geometrical configuration of 3D vector-FMR experiment measured at fixed frequency $\boldsymbol{f} = 20$ GHz. (b) Numerical calculation of the total free-energy function for in-plane magnetic field using the spin-only value $\boldsymbol{g} = 2$ (black) and angular value $\boldsymbol{g}(\theta_H)$ (red), where $\boldsymbol{\theta}$ is the polar angle of the magnetization. (c) Angular dependence of the in-plane FMR spectra. (d), (e) Temperature scan of the FMR spectra. The insets show the geometrical configuration with the static magnetic field $\boldsymbol{H}$ perpendicular (d) or parallel (e) to the rf field $\boldsymbol{H}_{\rm rf}$, and the internal effective field $\boldsymbol{H}_{\rm eff}$ slightly off the basal plane around $\boldsymbol{T_c}$. The anomalously parallel pumped single-domain mode (e) around the $\boldsymbol{T_c}$ originates from the nonvanishing effective field in the c axis, in contrast to the normally perpendicular pumped single-domain mode (d). Dashed lines are guides to the eye. And, $\omega/\gamma_{\rm spin}$ denotes the corresponding $\boldsymbol{H}_{\rm res}$ for a free spin at 20 GHz.

D. Anomalously parallel pumped excitations

In considering the large variation of g factor near T_c, the total free energy containing the anisotropic Zeeman energy $-\mu_{\rm B} H g \sum_j S_j$ thus should be modified. As shown in Fig. 4(a), we keep the magnetic field rotating in the basal plane. In Fig. 4(b), the total free energy for 35 K and 1 T ($H \parallel ab$ plane) is constructed with isotropic and anisotropic g factor, respectively. As we can see, the minimum position of $F(\theta)$ split off, where θ is the polar angle of the magnetization. It means the equilibrium angle of internal effective field $H_{\rm eff}$, which is determined by the minimum value of F (where $\partial F/\partial\theta_H = 0$), clearly deviates from basal plane ($\theta = 90^\circ$).

Generally, above the saturation field, the uniform single-domain mode with the wave vector $q = 0$ cannot be detected when the static field H is parallel to the microwave field $H_{\rm rf}$ [29]. More specifically, for the necessary moment of force driving Larmor precession, the internal effective field $H_{\rm eff}$ should have nonvanishing perpendicular component to $H_{\rm rf}$. Therefore, it is interesting to predict the anomalously parallel pumped FMR signals near the critical temperature can be excited due to anisotropic critical fluctuations:

$$\left(\frac{\omega}{\gamma}\right)^2 = (H_{\rm eff})^2[\cos^2\theta_{H_{\rm eff}} + \sin^2\theta_{H_{\rm eff}}\sin^2\phi_{H_{\rm eff}}]. \quad (8)$$

Therefore, the angular-dependent FMR spectra for in-plane rotation in Fig. 4(c) can be well explained by Eq. (8), which clearly shows the nonvanishing parallel pumped FMR signal. In addition, Figs. 4(d) and 4(e) show more clearly the perpendicular and parallel pumped FMR spectra above and below T_c. Two branches of multidomain and single-domain modes are observed on both sides of the saturation field. As for the parallel pumped FMR spectra, the observed single-domain mode at 20 GHz presents a saddle shape near T_c. Below T_c, the anisotropic Zeeman splitting gradually becomes isotropic, and thus the FMR signal fades away as approaching the saturation field.

E. Field effect and scaling of g shift

Because the FMR experiment is performed under finite magnetic field, there should be an effect on the field suppression of magnetic fluctuations. In fact, in considering the high-temperature perturbation in the Nagata theory, the criterion for the good approximation of Eq. (4) is that $g\mu_{\rm B} H\langle S^z\rangle \ll kT$. By varying the upper fitting field of ω–H at different temperature, we can therefore extract the field dependence of percent g shift in Fig. 5. We can clearly see that for temperatures well separated from T_c where the effect of magnetic fluctuations is small, the g shift is almost

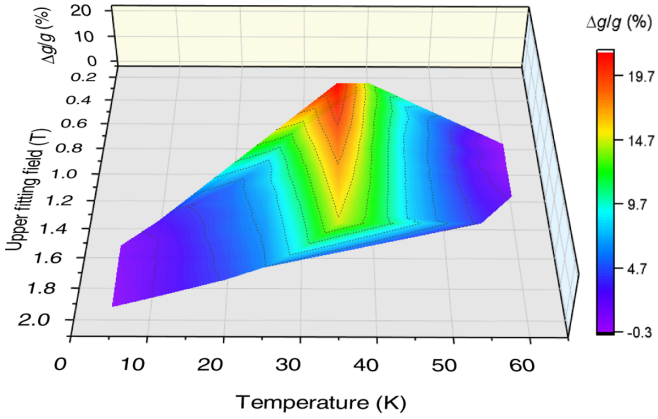

FIG. 5. The 3D color map of the field dependence of percent g shift. The fitted values of g factor are compared with the upper fitting field for the in-plane FMR spectra above the saturation field and at various temperature.

independent of the magnitude of the external magnetic field. However, as approaching T_c, the fluctuations become very large. The g shift decreases monotonically with the increase of the external magnetic field. We can reasonably infer that the g factor tends to approach the spin-only value $g = 2$ after the fluctuation is gradually suppressed under higher external magnetic field. In other words, the external field supports ferromagnetic ordering and can shift T_c to a higher temperature.

In the paramagnetic state above T_c, Nagata theory predicts a linear scaling of g shift with susceptibility [16]. The key procedure is substituting the correlation function by fluctuation-dissipation theorem, where $\langle S_z \rangle = \chi_{\mathrm{mol}}(T)H/N_A g\mu_B$ [$\chi_{\mathrm{mol}}(T)$ is the molar susceptibility, N_A is the Avogadro constant]. In the ferromagnetic state, although there is still lacking exact theory of critical dynamics below T_c, in considering the spontaneous magnetization $M_s = ng\mu_B\langle S_z \rangle$ (n is the amount of spins per volume), we can make an analogy and get a similar relationship:

$$\frac{\Delta g_{ab}}{g} = \frac{\chi_{ab} - \chi_c}{\chi_{ab}} = \frac{M_{ab} - M_c}{M_{ab}}, \tag{9}$$

$$\frac{\Delta g_c}{g} = -\frac{\chi_c - \chi_{ab}}{2\chi_c} = -\frac{M_c - M_{ab}}{2M_c}. \tag{10}$$

As a consequence of the field suppression of magnetic fluctuations, it seems difficult to scale the field dependence of g shift due to lacking the knowledge of correlation functions at finite magnetic field. However, above and below T_c where the g shift is hardly affected by magnetic field, we can extend the scaling of Eq. (9) and Eq. (10) to the static critical behavior at zero field. Therefore, by means of a modified Arrott plot, we extract the susceptibilities and spontaneous magnetization through isothermal magnetization. The determined critical exponents ($\beta = 0.169$, $\gamma = 1.489$) are close to the 2D Ising universality class [27,34]. As shown in Figs. 6(a) and 6(b), in a temperature range slightly deviating from T_c, the scaled g shift fits well with Eq. (9) and Eq. (10) for both in-plane and out-of-plane direction. However, in the extreme vicinity of T_c, the overestimation of Eq. (9) and Eq. (10) indicates the lack of classical spin approximation of Nagata theory.

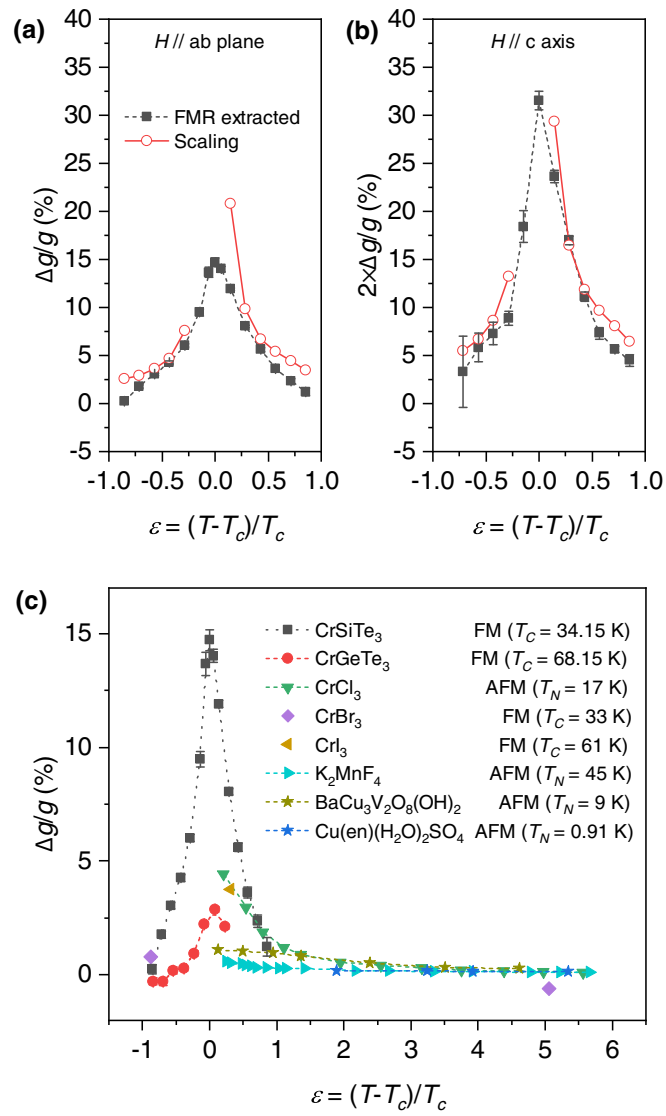

FIG. 6. (a), (b) Scaling of FMR extracted g shift by susceptibilities and spontaneous magnetization obtained from magnetometry measurements for in-plane and out-of-plane directions. (c) Comparison of the temperature dependence of g shift with that for typical 2D and quasi-2D ferromagnets ($CrSiTe_3$, $CrGeTe_3$ [27], $CrBr_3$ [30], and CrI_3 [28]) and antiferromagnets ($CrCl_3$ [31], K_2MnF_4 [16], $BaCu_3V_2O_8(OH)_2$ [32], and $Cu(en)(H_2O)_2SO_4$ [33]).

Maeda *et al.* showed involving the quantum fluctuations at finite temperature and magnetic field could give a better fitting to g shift [35]. Therefore, as we can see for the recent reported pressure-induced superconductivity [8] and possible Kitaev quantum spin liquid in strained monolayer $CrSiTe_3$ [4], the role played by strongly correlated quantum fluctuations cannot be ignored in this material.

Furthermore, we compare the g shift among the typical 2D and quasi-2D ferromagnets and antiferromagnets in Fig. 6(b). The giant g shift in an exceptionally wide critical window of $CrSiTe_3$ seems conspicuous compared to other magnetic 2D materials. The strong intrinsic magnetic fluctuations are of importance to the degeneracy of the ground state and also to mediating the formation of hidden quantum phases.

Therefore, $CrSiTe_3$ has the potential of quantum materials to be tuned by external perturbations, which needs further exploration.

IV. CONCLUSION

In conclusion, we systematically illustrate the effects of anisotropic critical fluctuations on the critical spin dynamics of 2D magnet. Such anisotropic g shift arises from both anisotropic spin interactions and critical fluctuations, which should happen universally in 2D magnetism and dominate at a wide critical window around T_c. As we extend Nagata theory to ferromagnetic state, the angle dependence of g factor above and below T_c shows excellent agreement with the FMR experiment. As a result of g shift, we find the anisotropic Zeeman splitting yields parallel pumped excitations around T_c. The amplitude of g shift is also strongly dependent on magnetic field that suppresses the critical fluctuations. Furthermore, our scaling of g shift with the static susceptibilities and spontaneous magnetization also reveals the validity of the theory. We hope our results can provide renewed insights on fluctuation-driven spin dynamics for 2D magnetism.

ACKNOWLEDGMENTS

This work was supported by the National Key R&D Program of China (Grants No. 2021YFB3501402 and No. 2017YFA0302901), National Natural Science Foundation of China (Grant No. 11974406), and Strategic Priority Research Program (B) of the Chinese Academy of Sciences (CAS) (Grant No. XDB33000000), and the Youth Innovation Promotion Association CAS (Grant No. 2021004). We thank Professor Wei Han, Professor Shiliang Li, Professor Yisheng Chai, and Dr. Wenshan Hong for the fruitful discussion.

[1] J. Als-Nielsen and R. J. Birgeneau, Am. J. Phys. **45**, 554 (1977).
[2] N. D. Mermin and H. Wagner, Phys. Rev. Lett. **17**, 1133 (1966).
[3] C. Xu, J. Feng, H. Xiang, and L. Bellaiche, npj Comput. Mater. **4**, 57 (2018).
[4] C. Xu, J. Feng, M. Kawamura, Y. Yamaji, Y. Nahas, S. Prokhorenko, Y. Qi, H. Xiang, and L. Bellaiche, Phys. Rev. Lett. **124**, 087205 (2020).
[5] L. Chen, J.-H. Chung, T. Chen, C. Duan, A. Schneidewind, I. Radelytskyi, D. J. Voneshen, R. A. Ewings, M. B. Stone, A. I. Kolesnikov, B. Winn, S. Chi, R. A. Mole, D. H. Yu, B. Gao, and P. Dai, Phys. Rev. B **101**, 134418 (2020).
[6] F. Zhu, L. Zhang, X. Wang, F. J. dos Santos, J. Song, T. Mueller, K. Schmalzl, W. F. Schmidt, A. Ivanov, J. T. Park, J. Xu, J. Ma, S. Lounis, S. Blgel, Y. Mokrousov, Y. Su, and T. Brckel, Sci. Adv. **7**, eabi7532 (2021).
[7] K. S. Burch, D. Mandrus, and J.-G. Park, Nature (London) **563**, 47 (2018).
[8] W. Cai, H. Sun, W. Xia, C. Wu, Y. Liu, H. Liu, Y. Gong, D.-X. Yao, Y. Guo, and M. Wang, Phys. Rev. B **102**, 144525 (2020).
[9] C. Gong, L. Li, Z. Li, H. Ji, A. Stern, Y. Xia, T. Cao, W. Bao, C. Wang, and Y. Wang, Nature (London) **546**, 265 (2017).
[10] M. Farle, Rep. Prog. Phys. **61**, 755 (1998).
[11] L. P. Kadanoff, W. Götze, D. Hamblen, R. Hecht, E. A. S. Lewis, V. V. Pal-Ciauskas, M. Rayl, J. Swift, D. Aspnes, and J. Kane, Rev. Mod. Phys. **39**, 395 (1967).
[12] P. C. Hohenberg and B. I. Halperin, Rev. Mod. Phys. **49**, 435 (1977).
[13] K. Nagata, Physica B+C **86**, 1283 (1977).
[14] K. Nagata, Y. Tazuke, and K. Tsushima, J. Phys. Soc. Jpn. **32**, 1486 (1972).
[15] K. Nagata and Y. Tazuke, J. Phys. Soc. Jpn. **32**, 337 (1972).
[16] K. Nagata, I. Yamamoto, H. Takano, and Y. Yokozawa, J. Phys. Soc. Jpn. **43**, 857 (1977).
[17] S. Khan, C. W. Zollitsch, D. M. Arroo, H. Cheng, I. Verzhbitskiy, A. Sud, Y. P. Feng, G. Eda, and H. Kurebayashi, Phys. Rev. B **100**, 134437 (2019).
[18] D. MacNeill, J. T. Hou, D. R. Klein, P. Zhang, P. Jarillo-Herrero, and L. Liu, Phys. Rev. Lett. **123**, 047204 (2019).
[19] V. Carteaux, F. Moussa, and M. Spiesser, Europhys. Lett. **29**, 251 (1995).
[20] Y. Liu and C. Petrovic, Phys. Rev. Mater. **3**, 014001 (2019).
[21] A. Aharoni, J. Appl. Phys. **83**, 3432 (1998).
[22] E. Frey and F. Schwabl, Adv. Phys. **43**, 577 (1994).
[23] D. L. Huber, Mod. Phys. Lett. B **26**, 1230021 (2012).
[24] M. Gibertini, M. Koperski, A. F. Morpurgo, and K. S. Novoselov, Nat. Nanotechnol. **14**, 408 (2019).
[25] D.-H. Kim, K. Kim, K.-T. Ko, J. H. Seo, J. S. Kim, T.-H. Jang, Y. Kim, J.-Y. Kim, S.-W. Cheong, and J.-H. Park, Phys. Rev. Lett. **122**, 207201 (2019).
[26] H. Beljers and J. Smit, Phil. Res. Rep **10**, 113 (1955).
[27] See Supplemental Material at http://link.aps.org/supplemental/10.1103/PhysRevB.106.054427 for FMR spectra, susceptibilities and spontaneous magnetization for $CrSiTe_3$. FMR spectra and extracted g factor for $CrGeTe_3$ as a comparison.
[28] I. Lee, F. G. Utermohlen, D. Weber, K. Hwang, C. Zhang, J. van Tol, J. E. Goldberger, N. Trivedi, and P. C. Hammel, Phys. Rev. Lett. **124**, 017201 (2020).
[29] Y. Onose, Y. Okamura, S. Seki, S. Ishiwata, and Y. Tokura, Phys. Rev. Lett. **109**, 037603 (2012).
[30] C. L. Saiz, J. A. Delgado, J. van Tol, T. Tartaglia, F. Tafti, and S. R. Singamaneni, J. Appl. Phys. **129**, 233902 (2021).
[31] S. Chehab, J. Amiell, P. Biensan, and S. Flandrois, Physica B **173**, 211 (1991).
[32] A. Zorko, F. Bert, A. Ozarowski, J. van Tol, D. Boldrin, A. S. Wills, and P. Mendels, Phys. Rev. B **88**, 144419 (2013).
[33] R. Tarasenko, A. Orendáčová, E. Čižmár, S. Maťaš, M. Orendáč, I. Potočňák, K. Siemensmeyer, S. Zvyagin, J. Wosnitza, and A. Feher, Phys. Rev. B **87**, 174401 (2013).
[34] B. Liu, Y. Zou, L. Zhang, S. Zhou, Z. Wang, W. Wang, Z. Qu, and Y. Zhang, Sci. Rep. **6**, 33873 (2016).
[35] Y. Maeda, K. Sakai, and M. Oshikawa, Phys. Rev. Lett. **95**, 037602 (2005).